Infotech Aerospace,26 - 29 September 2005, Arlington, Virginia AIAA2005-7171

Investigation of Variable Wing-Sweep for Applications in Micro Air Vehicles

J. Hall*, K. Mohseni†, D. Lawrence‡,
Research and Engineering Center for Unmanned Vehicles,
Department of Aerospace Engineering,
University of Colorado, Boulder, CO 80309-429.

P. Geuzaine§
CENAERO, Avenue Jean Mermoz 30, 6041 Gosselies, Belgium.

Micro Air Vehicles (MAVs) are noted for their small size and low-Reynolds number flight regime. Because they have small mass, they are attractive for use in sensing of toxic plumes. This mission requires high aerodynamic efficiency and the ability to be quickly and easily launched. A variable-sweep wing is investigated to meet these goals. Numerical simulations are used to demonstrate that sweeping the wings can provide plausible drag characteristics over a range of flight speeds. By sweeping the wing from 15° to 65°, L/D is improved by a factor of 2.6 at high speeds. This is caused by a decrease in parasitic drag corresponding to increased sweep angle.

I. Introduction

Micro Air Vehicles (MAVs) are small aircraft with potential applications ranging from surveillance and communication to sensor networks in both civilian and military applications. MAVs are distinguished by their small size and their often unknown aerodynamic characteristics. Because MAVs operate in a flow regime with Reynolds number below 200,000 they behave much differently than conventional aircraft. At these low Reynolds numbers, the ratio of lift to drag is significantly lower than that of large-scale aircraft. Also, laminar separation bubbles and unsteady effects contribute significantly to the aircraft's performance.

MAV aerodynamics have been received increased attention over the past decade. Ifju *et al.*[1] have studied the behavior of flexible wings and the use of a 2D coupled Navier-Stokes and structural solver for membrane wings. Lian *et al.*[2] developed numerical techniques for solving the fluid-structure interaction of a membrane wing using a moving grid. They reported on the size and location of separation bubbles for low AR wings at low Reynolds numbers, as well as the effect of end plates on tip vortices. Others have investigated control aspects for MAVs. Mueller and DeLaurier[3] reviewed various aspects of MAV aerodynamics. They discussed the deterioration of performance as Reynolds number decreases below 500,000 due to laminar separation and also described the "separation bubble." For $Re > 50,000$, the shear layer behind the separation point could induce turbulence, re-energizing the boundary layer and causing the flow to reattach to the surface. The size and location of the separation bubble can have a great impact of the performance of the vehicle.

Another issue with MAVs is the effect of freestream turbulence. Typical flight speed is on the order of 20 mph, meaning that a wind gust can increase relative airspeed by 50-100%. This increase in Reynolds

*Graduate student, AIAA member.
†Assistant Professor, AIAA member. Corresponding author mohseni@colorado.edu
‡Associate Professor, AIAA Member
§Group Leader, AIAA member.

number and dynamic pressure causes a large instantaneous increase in wing loading and may cause structural damage. The use of flexible membrane wings allows the MAV to decrease camber and hence lift coefficient in response to a large wind gust, alleviating some of the adverse effects of the gust.[1]

This paper will report on the application of variable-sweep high AR wings to MAVs. Section II gives an overview of the current project and applications. Section III introduces the concept of a variable-sweep wing and the aerodynamic properties of interest. Section IV describes the model used for numerical simulations, while Section V outlines the numerical technique and Section VI covers validation of the numerical results. Section VII provides results and analysis from the simulations, and Section VIII contains concluding remarks.

II. Project Description

The goal of the Colorado MAV project is to develop a MAV as a sensor platform for investigation of plumes of hazardous contaminants.[4] In the event of an industrial disaster or terrorist attack, dangerous chemicals and/or radioactive pollutants may be released into the lower atmosphere. Depending on wind conditions, the contaminants could spread over a large area or remain in one region. In order to predict and monitor the location of the plume, and initiate the proper emergency procedures, a method is needed for sensing contaminant levels in the atmosphere. A MAV network could provide a practical solution for several reasons including among others:[4,5]

1. MAVs are operated remotely, thus avoiding additional human health risks.
2. MAVs have small mass, reducing the risk to people and property on the ground in the event of failure.
3. MAVs are more maneuverable than balloons and may be deployed to actively track the regions of highest contaminant concentration.
4. MAVs can be produced cheaply and operated by a small team, making it possible to deploy a large flock ($\sim$100 vehicles) at a reasonable cost.
5. MAVs can be launched by a catapult mechanism, removing the need for an airport or runway.
6. MAVs are essentially invisible and silent a few meters away from their flight path. As a result they will not create public panic in the case of an emergency.

From this mission description, vehicle requirements can be derived. The MAV must be small, weighing approximately 200 g. It must be easily launched; for this purpose, the MAV will fold or collapse to enable tube launch. The MAV must be able to remain aloft for up to 120 minutes. To accomplish the duration goal, the aircraft should have the highest lift-to-drag ratio possible. Finally, the MAV must be able to travel rapidly to the location of the plume, then loiter at low speed. Loiter speed is about 8 m/s, while cruise speed is about 20 m/s.

A flexible wing MAV called CMAV has already been designed and built at the University of Colorado.[4] It represented the first generation of design concepts for the project. It was built with a low-AR flexible membrane wing supported by carbon fiber ribs and batons. The fuselage was also constructed of carbon fiber, and the vehicle was propelled by an electric motor.

The second generation CMAV will have similar construction, but different features. In order to improve the aerodynamic efficiency, the low-AR wing will be replaced by one with AR around 9. To facilitate the tube launch concept and maximize efficiency for both the high-speed dash and the low-speed loiter, a variable-sweep wing design will be implemented. The motor and propeller will be mounted in the rear to reduce damage during landings. The pusher configuration gives the propeller and motor greater protection during landings, and also increases stability. Another major change will be to relocate the batteries from the fuselage to the wings. They will be stored in a leading edge spar, to which the membrane and its baton supports will attach. Locating the batteries in the wings serves three purposes:

1. Decrease the size of the fuselage, reducing drag.
2. Shift weight to the wings, so that the C.G. can follow the center of lift more closely when sweeping the wings.
3. Decrease wing loading, which will reduce the size and weight of the sweeping mechanism.

III. Variable-Sweep Wing

Traditionally, variable sweep has been used to increase the critical Mach number of transonic and supersonic jets while providing low-speed maneuverability and decreased stall speed.[6] This technology also has potential applications in UAVs, despite the lack of compressibility effects. Variable-sweep wings were used on the UAV Aesalon, developed by a team at the University of Wisconsin-Madison.[7] At top flight speed, they reported a 10% reduction in drag as the sweep angle Λ increased from 10° to 50°. Neal *et al.*[8] constructed a morphing experiment to test different types of wing morphing, and they reported that minimum C_D actually increased slightly as the sweep angle increased, citing additional drag on the wing tips as a possible cause. Their tests were performed at $Re = 843,000$. To get an accurate description of the effect of variable sweep on aircraft performance in the low-Reynolds number regime of MAV flight, CFD analysis is required.

The equations for lift and drag are given by:[9]

$$\begin{aligned} D &= q_\infty C_D S; \\ L &= q_\infty C_D S; \\ C_D &= C_{D,0} + \frac{C_L^2}{\pi e AR}; \end{aligned} \tag{1}$$

where q_∞ is the dynamic pressure $\frac{1}{2}\rho_\infty U_\infty^2$, ρ_∞ and U_∞ are the density and velocity of the freestream, S is the reference area, L is the lift, D is the drag, C_D is the drag coefficient, C_L is the lift coefficient, AR is the aspect ratio, and e is the span efficiency factor, respectively. An example of the variation of total drag with velocity for a fixed sweep angle is shown in Figure 1. There is clearly a minimum value of drag, which occurs when $C_{D,0} = C_{D,i}$. The goal of variable sweep is to shift this minimum to higher velocity when the wings are swept back.

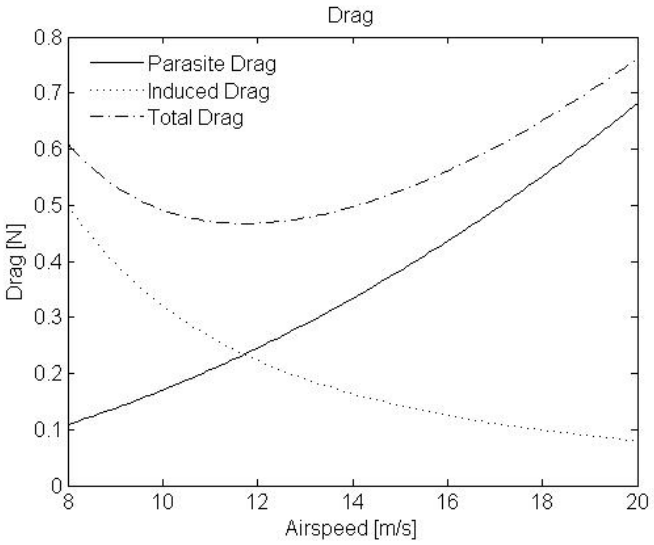

Figure 1. Example of relationship between drag components and airspeed

Combining Equations 2 and using the definitions of q_∞ and AR as well as the condition of lift equal weight ($L = W$) for level flight, we obtain

$$D = \frac{1}{2}\rho U_\infty^2 C_{D,0} S + \frac{2W^2}{\pi e \rho b_0^2 (U_\infty \cos\Lambda)^2} \tag{2}$$

The first term in the above equation represents the contribution of parasite drag. The second term represents the induced drag, which decreases with U_∞ but increases with Λ. In order to determine the value of Λ which gives the minimum drag, the relationships of $C_{D,0}$ and e with Λ must be determined.

IV. Model Description

To examine the effects of wing sweep, a simple CAD model was developed (Figure 2). Although not intended for production, the model was intended to be as realistic as possible and was designed to mimic the original CMAV[10] in mass and volume characteristics to facilitate comparison between the two. New aircraft concepts made the new vehicle much different, however. On the CMAV, the fuselage made a significant contribution to drag but not to lift. This has been avoided on the new model by relocating battery storage to the wings and making the fuselage smaller and flatter. The electric motor and propeller are mounted on a shaft protruding from the rear of the fuselage. The motor pod is extended from the fuselage to ensure propeller clearance with swept wings.

(a) 15° sweep angle

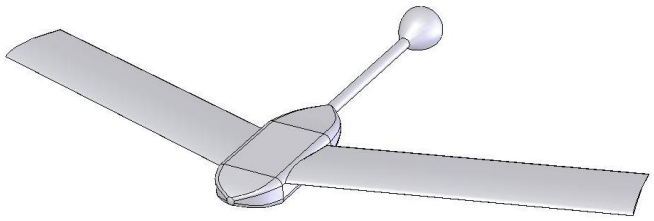

(b) 40° sweep angle

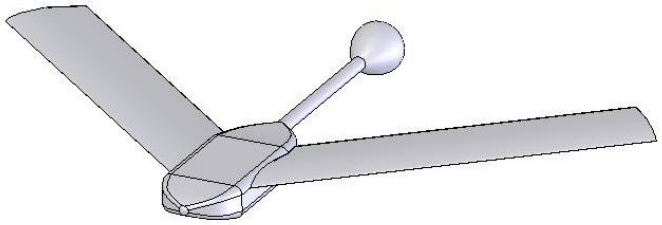

(c) 65° sweep angle

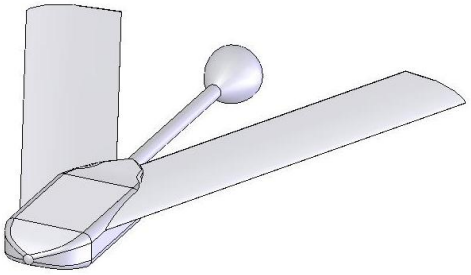

Figure 2. CAD model used for CFD simulations.

The wings have the same Eppler 387 airfoil as the Colorado MAV. A rectangular box with the approximate dimensions of the lithium-ion batteries is located near the leading edge, and a spline curve smoothly encases the box within the wing. Behind the box the wing tapers to a very thin section to represent a membrane wing. The wings are each 0.5 m long and have a 0.1 m chord. Three versions of the model were generated for $\Lambda = 15°$, $40°$, and $65°$.

V. Numerical Technique

Numerical flow simulations were used to determine the effect of variable wing sweep on a low-Reynolds number MAV. Waszak *et al.*[11] and Viieru *et al.*[12] have reported that the results for a rigid wing are very similar to those of a flexible wing at a much smaller computational cost; hence, this paper deals only with rigid wings. To simulate the flow around the MAV, the flow solver described in Mohseni *et al.*[4,10] was used on an eight-processor parallel computer. The CFD software was a domain decomposition-based parallel three-dimensional flow solver with capabilities for both the Euler and Navier-Stokes equations. The solver used a combination of finite volumes and finite elements for the spatial discretization. Spatial discretization was accomplished with an upwind scheme for the convective term and a Galerkin method for the diffusive term. The flow was integrated in time with a backward Euler scheme. To solve the system of nonlinear equations, a Newton method with finite difference GMRES solver and preconditioner was used.[10]

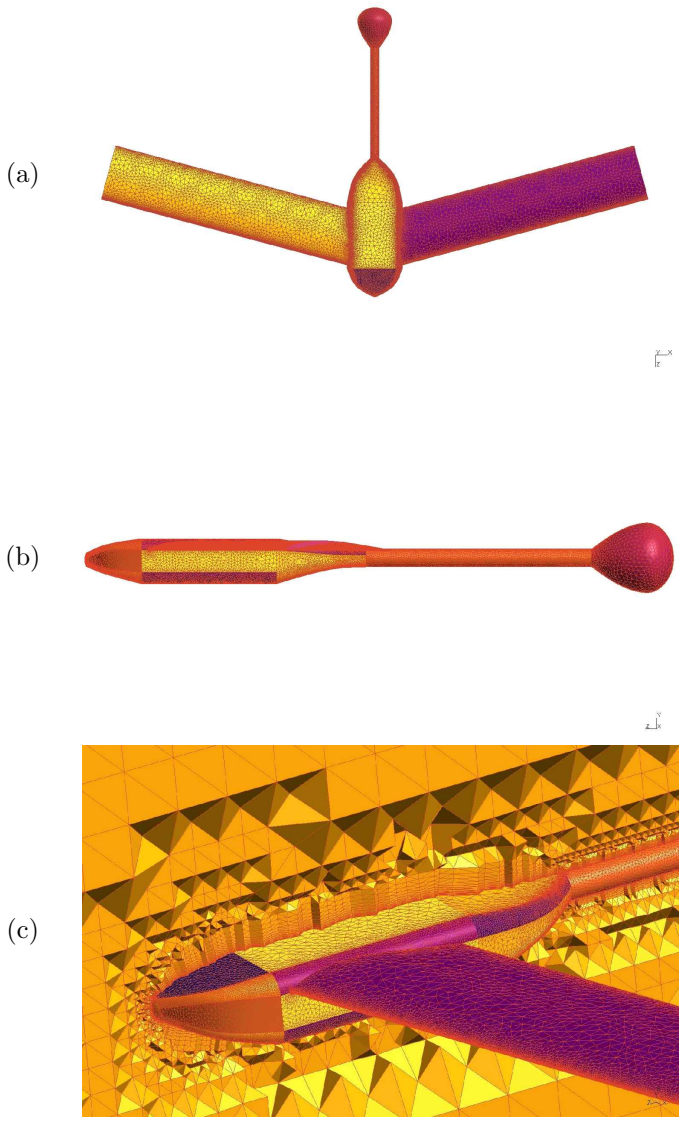

Figure 3. Computational grid applied to surface of MAV with 15° sweep. (a) top view, (b) side view, (c) cut through center of computational domain showing volume and boundary layer elements.

The CAD model was used to create a cavity in a much larger sphere. This sphere formed the computational domain. The mesh generator created an unstructured mesh. First, triangular elements were used to discretize the surfaces of the vehicle. The surface mesh was then refined in areas of high curvature, such as the leading edges of the wings. Next, stretched tetrahedral elements were formed near the surface of the vehicle to capture the effect of the boundary layer. The remaining volume was filled with tetrahedra. Finally, in a cylinder surrounding the vehicle the mesh was refined to more accurately compute the wake behind the vehicle. The resulting mesh had approximately 3.9 million elements (Figure 3).

VI. CFD Validation

To verify the accuracy of the results and the fidelity of the mesh, a second mesh was generated with higher resolution, composed of 6.9 million elements. The simulations for $\Lambda = 15°$ and 8 m/s were repeated with the new mesh, and the results were compared to the results for the original mesh (Figure 4). The validation simulations took between six and eight hours each to complete, as opposed to three to four hours for the original mesh. The results showed very little difference between the two meshes. The average absolute error was -0.020 for C_L (0.65% relative error) and 0.012 for C_D (7.9% relative error).

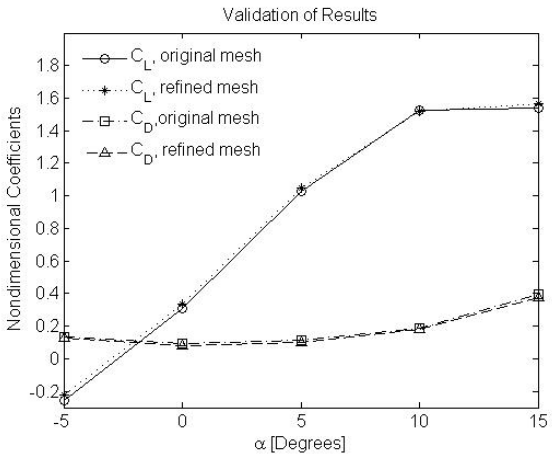

Figure 4. Comparison of results for vehicle with $\Lambda = 15°$ at 8 m/s on original and refined meshes.

VII. Results

Aerodynamic Coefficients. Flow simulations were run for several different scenarios. Each model was simulated at three values of far-field velocity U_∞ (8 m/s, 14 m/s, and 20 m/s) and five angles of attack α, ranging from -5° to 15° in 5° increments. The results were then tabulated and analyzed. Figure 5 displays the coefficients of lift and drag for each model at different velocities. The most obvious effect of sweep angle on C_L is the change in lift-curve slope. The slope is 0.12 per degree for 15° sweep, 0.08 for 40°, and 0.05 per degree for 65° sweep. The change in slope is caused by a decrease in the effective camber. When the wing is swept, the effective cord length becomes $c' = \frac{c}{\cos\Lambda}$. The total camber of the wing remains unchanged, resulting in a decreased percent camber of the wing and smaller lift-curve slope. The angle of attack which generates zero lift is -2.7° for 15° sweep, -2.5° for 40° sweep, and -0.1° for 65° sweep.

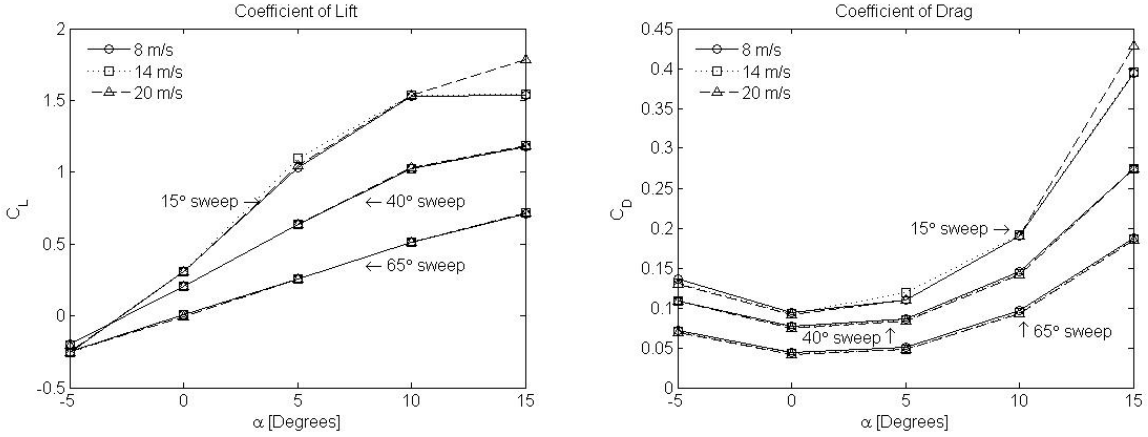

Figure 5. Aerodynamic coefficients for four different cases: (a) Lift Coefficient and (b) Drag Coefficient.

The coefficient of lift is essentially independent of velocity in the velocity range considered here. The only significant deviation is for the case of the aircraft with 15° sweep operating at $\alpha = 15°$, where $C_L = 1.6$ for 8 m/s and 1.8 for 20 m/s. In both cases, the flow has separated from the upper surface of the wing. Figure 6 shows that the separation point is closer to the leading edge at 20 m/s than at 8 m/s.

The swept configuration has a lower coefficient of drag, due to its smaller frontal profile. Parasitic drag coefficient $C_{D,0}$ for the fully swept configuration is less than half that of the unswept counterpart, 0.11 compared to 0.04. At 40° sweep the value lies in the middle at 0.08. The 15° sweep vehicle also has greater

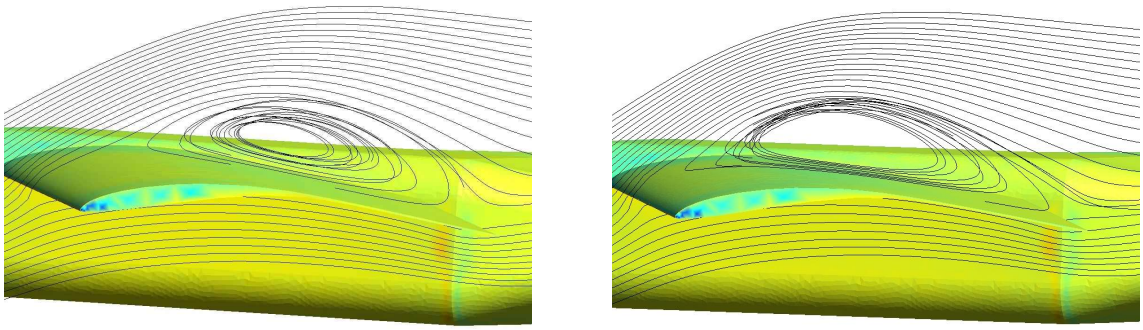

(a) (b)

Figure 6. Streamlines for the aircraft with 15° sweep at 15° angle of attack, freestream velocity of (a) 8 m/s and (b) 20 m/s.

induced drag due to the steeper lift curve.

The lift-to-drag ratio is critical for the MAV. In order to achieve long duration flight, the aircraft must be as efficient as possible. Figure 7 displays L/D versus α. For all three configurations, the most efficient α is around 5°.

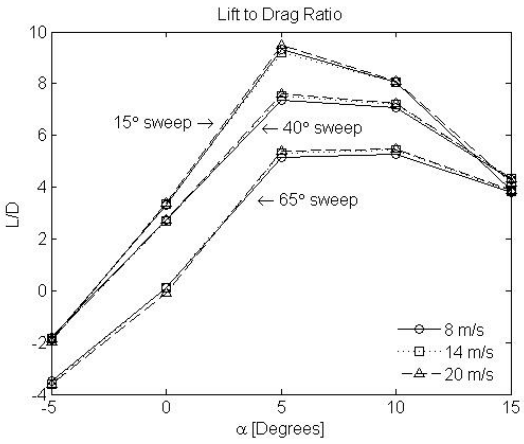

Figure 7. Lift-to-Drag ratio versus angle of attack.

Flight Characteristics. Level flight requires $L = W$, which is approximately 1.96 N for the MAV. Under this condition the lift coefficient is inversely proportional to the square of velocity, requiring a change in α for level flight. The relationships of C_D and L/D with airspeed provide insight into the effects of wing sweep. To find this relationship, the required lift coefficient was determined as a function of U_∞ from Equation 2. The α for level flight was then found by interpolation using the C_L curves for 14 m/s. A second interpolation with the C_D curves for 14 m/s yielded the drag coefficient. Finally, C_D and L/D were plotted as functions of U_∞ (Figure 8).

At low speed, the fully swept configuration has by far the greatest C_D. This is because of the high α needed to fly for that situation. As the airspeed increases, C_D for $\Lambda = 65°$ decreases until it is much less than the other two. From the plot of L/D, one can see that the fully swept wing is more efficient at nearly all speeds. The reason for this is that the wing is larger than necessary for a vehicle of 200 g. The light weight and large wing area cause the vehicle's operating point to be well away from the optimum L/D, which occurs around $\alpha = 5°$. To compensate and also gain better understanding of the effects of sweep, the wing area was decreased by half, and the relationships of C_D and L/D were recalculated.

Figure 8(d) shows the relationship of L/D with U_∞ after adjustment. As the speed increases, higher angles of sweep become more efficient. At the low speeds, 15° sweep provides the greatest L/D. As the speed increases to about 9.5 m/s, the 40° sweep wing becomes more efficient. The 65° sweep configuration takes over around 13 m/s. The most efficient flight can be determined by smoothly varying Λ with U_∞ in order to maximize L/D at every point.

The reason for the change is the combined effect of parasite and induced drag. For example, at 8 m/s the swept wing vehicle requires $C_L = 0.59$ to fly. Recall from Equation 2 that induced drag is proportional to C_L^2. Increasing speed to 20 m/s causes a decrease in C_L to 0.094, significantly dropping the induced drag from its low speed value. Parasite drag, which is proportional to $C_{D,0}U_\infty^2$, thus becomes the dominant effect at high speed. Since $C_{D,0}$ for 65° sweep is less than half of that for 15° sweep, the fully swept configuration has lower parasite drag and hence total drag at high speed. At low speed, the 15° sweep wing produces less

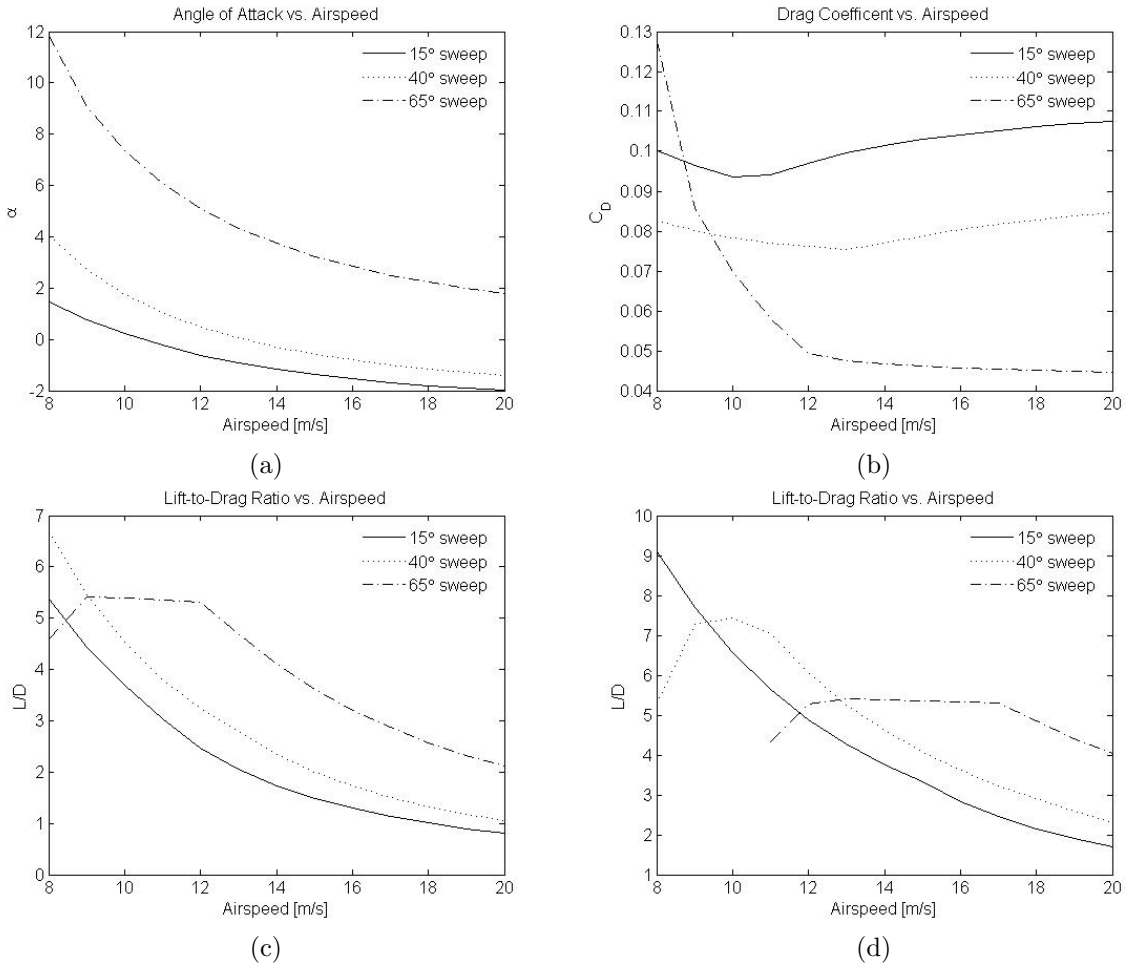

Figure 8. Variation with airspeed for level flight: (a) α, (b) C_D, (c) L/D, and (d) L/D for adjusted wing area.

induced drag and is therefore more efficient.

Separation Bubble and Boundary Layer Effects. The separation bubble is less noticeable than on the CMAV, and often nonexistent. Whereas the CMAV simulations reveal a laminar separation of the flow near the leading edge which reattached to the wing surface before reaching the trailing edge,[10] the current simulations show separation at a delayed point on the wing surface. Reattachment occurs just before the trailing edge, or not at all. Figure 9 shows the boundary layer and separation zones for two different cases.

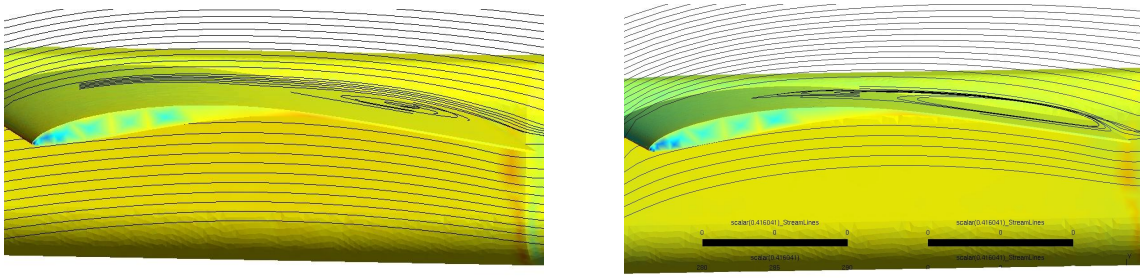

(a) (b)

Figure 9. (a) Streamlines and separation zone for unswept configuration at $\alpha = 5°$ and 8 m/s. (b) Same for $\alpha = 10°$s.

The most likely cause for the difference in behavior between the new design and the CMAV is the change in AR. The CMAV had a low AR wing with a non-rectangular planform, while the new design features high AR and rectangular planform. Because of the shorter chord, the flow has less distance to reattach once it separates. Another possible factor is the airfoil; although the same airfoil shape was used, the camber was greater. This could delay the separation to a further point in the streamwise direction.

As the sweep angle increases, the behavior of the boundary layer and separation change as well. For small sweep angles, there is a separation starting around the $\frac{1}{2}$ chord point. The strength of the recirculation zone weakens with increased sweep angle, and the streamlines take on a greater spanwise component of velocity. According to Kuethe and Chow,[13] a strong component of pressure gradient in the spanwise direction gives the flow a radius of curvature in that direction. This is seen as an S-like curve of the streamlines (Figure 10). The curvature is greatest at the surface of the wing. At $\Lambda = 65°$, a separation bubble forms near the leading edge. Because of the strong flow component parallel to the leading edge, the streamlines spiral out toward the tip.

VIII. Conclusion

The use of variable sweep to improve MAV flight characteristics over a wide range of airspeed is found to be beneficial. A decrease in parasite drag due to a smaller frontal profile results in decreased drag at high speeds. By sweeping the wings from 15° to 65°, C_D can be reduced by nearly 60% for airspeed of 20 m/s. It is possible to achieve $L/D > 9$ at 8 m/s and $L/D > 5$ at 20 m/s.

References

[1]P.G. Ifju, D.A. Jenkins, S. Ettinger, Y. Lian, W. Shyy, and M.R. Waszak. Flexible-wing-based micro air vehicles. AIAA paper 2002-0705, January 2002. 40^{th} Aerospace Sciences Meeting & Exhibit, Reno, Nevada.

[2]Y. Lian, W. Shyy, D. Wiieru, and B. Zhang. Membrane wing aerodynamics for micro air vehicles. *Prog. in Aero. Sci.*, 39(6-7):425–465, 2003.

[3]T.J. Mueller and J.D. Delaurier. Aerodynamics of small vehicles. *Ann. Rev. Fluid Mech.*, 35:89–111, 2003.

[4]K. Mohseni, D. Lawrence, D. Gyllhem, M. Culbreth, and P. Geuzaine. Flow simulation around a micro air vehicle in a plume characterization scenario. AIAA paper 2004-6598, American Institute of Aeronautics and Astronautics, *3rd* Unmanned Unlimited Technical Conference, Workshop and Exhibit, September 20-22 2004.

[5]D.A. Lawrence, K. Mohseni, and R. Han. Information energy for sensor- reactive UAV flock control. AIAA paper 2004-6530, Chicago, Illinois, 20-23 September 2004. 3rd AIAA Unmanned Unlimited Technical Conference, Workshop and Exhibit.

[6]J.D. Anderson Jr. *Introduction to Flight, Third Ed.* McGraw Hill, Boston, MA, 1989.

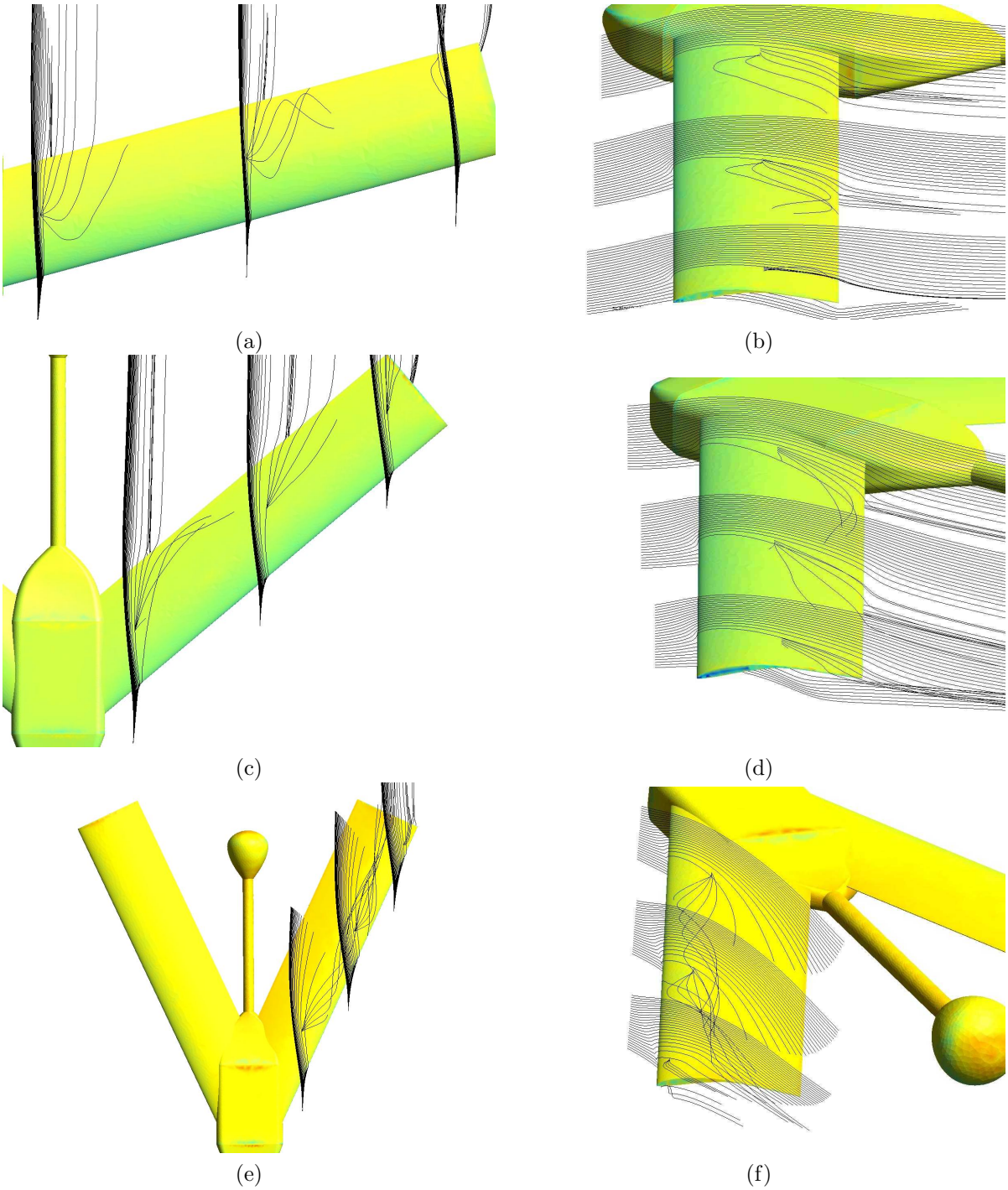

Figure 10. Streamlines for 14 m/s and $\alpha = 10°$. (a) $\Lambda = 15°$, top view; (b) same for end view; (c) $\Lambda = 40°$, top view; (d) same for end view; (e) $\Lambda = 65°$, top view; and (f) same for end view.

[7]Project merlin. University of Wisconsin College of Engineering, August 2005. http://homepages.cae.wisc.edu/∼floatn/merlin/project.htm.

[8]D.A. Neal, M.G. Good, C.O. Johnston, H.H. Robertshaw, W.H. Mason, , and D.J. Inman. Design and wind-tunnel analysis of a fully adaptive aircraft configuration. AIAA paper 2004-1727, American Institute of Aeronautics and Astronautics, *45th* structures, Structural Dynamics and Materials Conferencet, April 19-22 2004.

[9]J.D. Anderson Jr. *Fundamentals of Aerodynamics*. McGraw Hill, New York, NY, 2001.

[10]D. Gyllhem, K. Mohseni, D. Lawrence, and P. Geuzaine. Numerical simulation of flow around the Colorado micro aerial vehicle. AIAA paper 2005-4757, American Institute of Aeronautics and Astronautics, *35th AIAA Fluid Dynamics Conference and Exhibit*, Toronto, Canada, June 6-9 2005.

[11]M.R. Waszak and L.N. Jenkins. Stability and control properties of an aeroelastic fixed wing micro aerial vehicle. AIAA paper 2001-4005, August 2001. AIAA Atmospheric Flight Mechanics Conference, Montreal, Canada.

[12]D. Viieru, Y. Lian, W. Shyy, and P.G. Ifju. Investigation of tip vortex on aerodynamic performance of a micro air vehicle. AIAA paper 2003-3597, 2003.

[13]A.M. Kuethe and C.Y. Chow. *Foundations of Aerodynamics: Bases of Aerodynamic Design*. John Wiley and Sons, Inc., New York, NY, 1998.